IEEE Access
Multidisciplinary ⋮ Rapid Review ⋮ Open Access Journal

Received 30 December 2022, accepted 11 January 2023, date of publication 13 January 2023, date of current version 19 January 2023.

Digital Object Identifier 10.1109/ACCESS.2023.3236813

RESEARCH ARTICLE

Broadband S-Parameter Simulation Based on the Mixed Finite-Element Method and Symmetric Lanczos Algorithm

KE CHEN[1], (Member, IEEE), JUNHUI CHEN [1], XUANYING HOU[1], MINGWEI ZHUANG[1], (Member, IEEE), AND QING HUO LIU[1,2], (Fellow, IEEE)

[1]Institute of Electromagnetics and Acoustics, Xiamen University, Xiamen 361005, China
[2]Eastern Institute for Advanced Study, Ningbo 315200, China

Corresponding authors: Mingwei Zhuang (mw.zhuang@xmu.edu.cn) and Qing Huo Liu (qhliu@eias.ac.cn)

This work was supported by the National Natural Science Foundation of China under Grant 62101470 and Grant 61871462.

ABSTRACT In this paper, the symmetric Lanczos algorithm and mixed finite element method are combined to improve the efficiency and accuracy of S-parameter simulation in a broad frequency band. The mixed finite element method based on tree-cotree splitting is adopted to overcome the low-frequency (high-density) breakdown problem, thus ensuring the accuracy of low frequency (high integration density) results. The modified symmetric Lanczos algorithm for second order eigenvalue problem is employed for fast frequency sweep by one matrix inversion, then the field in the entire frequency band is obtained rapidly by solving the reduced order matrix equation. The accuracy of the high frequency results is improved by increasing the number of Lanczos vectors. Numerical simulations of two integrated passive filters (IPD filter) and an interconnect model are shown to verify the hybrid method along with commercial software HFSS.

INDEX TERMS Symmetric Lanczos algorithm, fast frequency sweep, low-frequency breakdown, mixed finite-element method (MFEM).

I. INTRODUCTION

In the signal integrity analysis of large-scale integrated circuits, it is often necessary to extract S-parameters in a wide frequency band for interconnects, packages, and chips, since S-parameters are the basis of link simulations. The traditional frequency sweep method based on FEM is time-consuming because it repetitively solves large systems of EM equations at many frequency points, so it is not suitable for wide-band PCB-level and system-level electromagnetic simulation. Model order reduction (MOR) techniques [1], [2], [3] transform a larger system into an approximate smaller system, which can significantly improve the solution efficiency with a high degree of accuracy. Among the MOR techniques, the Krylov subspace method based on Lanczos algorithm [4] is widely used in modal analysis, complex eigenvalue analysis, frequency domain response analysis and linear system problems. Compared with the asymptotic waveform evaluation (AWE) method [5], [6], [7], [8], [9], the Lanczos algorithm can search for all zeros and poles of the transfer function in a wide band. Lanczos algorithm was originally used to solve eigenvalue problems. A great deal of research has focused on combining the Lanczos algorithm with the full-wave algorithm for fast frequency sweep analysis. In [10], the symmetric and asymmetric Lanczos algorithm combined with FEM method are employed to analyze damped dynamic problems. In this paper, the system of second order differential equations is transformed into a first order system with twice the size. Reference [11] discusses a compromise technique to maintain semiorthogonality in the nonsymmetric Lanczos method, which turns to be more efficient than Arnoldi's algorithm. In [12], for the passive and lossless dielectric waveguides, a fast frequency sweep technique based on the constrained Lanczos algorithm and AWE is proposed. Then Sun et. al. [13], [14] applies the adaptive Lanczos-Padé Spectral method to the mixed-potential integral equation and FEM equation for broadband electromagnetic field analysis. Reference [15] uses the mass lumping

The associate editor coordinating the review of this manuscript and approving it for publication was Guido Lombardi.

technology to extend the Lanczos algorithm in time-domain and frequency-domain finite element to analyze electromagnetic field problems in lossless media. Then in [16], matrix-Padé via Lanczos (MPVL) is extended to model multiple-input multiple-output systems by using the finite element method. Recently, reference [17] applies Lanczos algorithm to speed up the EM sensitivity analysis over a frequency range.

Among the above methods, the high frequency error can be improved by increasing the number of Lanczos vectors, but the low frequency simulation will still face the low-frequency breakdown problem [18], [19], [20], [21], [22]. In addition, this problem occurs when the mesh size of the object is much smaller than the wavelength corresponding to the operating frequency. The problem is becoming increasingly prominent in the electromagnetic simulation of 3D large-scale integrated circuits when the chip becomes more and more complex and the technology node is pushed to the nanometer level (thus is may be also called the ''high-density breakdown'' problem). The current mainstream commercial softwares such as COMSOL, HFSS, and CST suffer from the low-frequency breakdown problem in their 3D full-wave algorithms. The fundamental reason for the low-frequency breakdown is that the divergence of electric field cannot be constrained in the traditional methods, resulting in pseudo-zero modes in spectral decomposition of the system matrix. A large amount of research shows that the mixed finite element method (MFEM) and the mixed spectral element method (MSEM) can effectively overcome the low-frequency breakdown problem. The MFEM and MSEM method can be implemented in two ways: one is based on the null-space theory of the stiffness matrix and the tree-cotree splitting technique [21], [22], [23], [24], [25], [26], and the other is based on the Lagrange multiplier technique [20], [27], [28] [29], [30]. The results show that the former can achieve the same accuracy as the latter with fewer degrees of freedom, although with an additional step of tree-cotree splitting.

To solve the low-frequency (high-density) breakdown problem caused by fine and complex structures and the problem of large-scale computation in wide frequency band in integrated circuits, we combine the mixed finite element method (MFEM) with the fast frequency sweep method (the symmetric Lanczos method). Although neither the MFEM nor the fast frequency sweep method is new, their combination is new and is the main contribution of this work. The main difference between the combination method in this paper and the previous methods in [20], [25], and [26] is that a modal order reduction method is applied to the MFEM method based on tree-cotree splitting in frequency domain to calculate S parameters, while the previous papers [20], [25], and [26] proposed two different mixed finite element methods in time domain (MFETD) based on Lagrangian multiplier [20] and tree-cotree splitting [25], [26], respectively. The time-domain method can obtain S parameters by Fourier transform in a wide frequency band by one calculation. However, it always takes long runtime to attenuate energy to 0 to obtain correct S parameters. Traditional frequency-domain methods need to calculate S parameters at each frequency to obtain broadband information. In this paper, the modal order reduction technology is used to project a large-scale matrix equation into a small-dimensional subspace, which can significantly improve the computational efficiency of the frequency domain method, and the MFEM method based on tree-cotree splitting in this paper can overcome the low frequency breakdown problems for electrically small problems.

II. MFEM FORMULATION

In this section, the MFEM formulation based on tree-cotree splitting [25] for two kinds of EM equations in Laplace domain is derived. One contains only s or s^2 term, corresponding to diffusion equation and lossless wave equation, respectively. The other contains both s and s^2 terms when either bulk conductivity, first-order absorbing boundary conditions (ABC) or lumped resistors is considered.

In the MFEM formulation, the wave equation and electric field divergence constraint equation (Gauss's law) are solved simultaneously. The equations in the Laplace domain are given as follows:

$$\nabla \times (\mu^{-1}\nabla \times \mathbf{E}) + s^2\epsilon\mathbf{E} + s\sigma_e\mathbf{E} = -s\mathbf{J}_i \tag{1}$$

$$s^2\nabla \cdot (\epsilon\mathbf{E}) + s\nabla \cdot (\sigma_e\mathbf{E}) = -s\nabla \cdot \mathbf{J}_i \tag{2}$$

where $s = j\omega$. The electric field $\mathbf{E}$ is expanded by edge basis functions Φ_i^c and the gradient of nodal basis functions $\nabla\varphi_j$:

$$\mathbf{E} = \sum_{i=1}^{N_c} e_i^c \Phi_i^c + \sum_{j=1}^{N_n} e_j \nabla\varphi_j \tag{3}$$

where N_c and N_n are the number of cotree edges and free nodes, respectively. By using Galerkin's method and introducing the gradient matrix $\mathbf{G}$ defined in [25], equations (1) and (2) are written as the following discrete matrix equations:

$$s^2\mathbf{Me} + s\mathbf{Ce} + \mathbf{Ke} = -s\mathbf{b} \tag{4}$$

$$\mathbf{G}^T(s^2\mathbf{Me} + s\mathbf{Ce} + s\mathbf{b}) = 0 \tag{5}$$

where $\mathbf{M}$, $\mathbf{C}$ and $\mathbf{K}$ are the mass, damping and stiffness matrices, respectively, $\mathbf{b}$ is the column vector associated with the source. Their expressions are shown as follows:

$$\mathbf{M} = \begin{bmatrix} \mathbf{M}^{cc} & \mathbf{M}^{cp} \\ \mathbf{M}^{pc} & \mathbf{M}^{pp} \end{bmatrix} \tag{6}$$

$$\mathbf{C} = \begin{bmatrix} \mathbf{C}^{cc} & \mathbf{C}^{cp} \\ \mathbf{C}^{pc} & \mathbf{C}^{pp} \end{bmatrix} \tag{7}$$

$$\mathbf{K} = \begin{bmatrix} \mathbf{K}^{cc} & \mathbf{0} \\ \mathbf{0} & \mathbf{0} \end{bmatrix} \tag{8}$$

$$\mathbf{b} = \begin{bmatrix} \langle \Phi^c, \mathbf{J}_i \rangle_\Omega \\ \langle \nabla\varphi, \mathbf{J}_i \rangle_\Omega \end{bmatrix} \tag{9}$$

where $\mathbf{M}^{cc}$ and $\mathbf{C}^{cc}$ are in the form of $\langle \Phi^c, a\Phi^c \rangle_\Omega$, $\mathbf{M}^{cp}$ and $\mathbf{C}^{cp}$ are in the form of $\langle \Phi^c, a\nabla\varphi \rangle_\Omega$, $\mathbf{M}^{pc}$ and $\mathbf{C}^{pc}$ are in the form of $\langle \nabla\varphi, a\Phi^c \rangle_\Omega$, $\mathbf{M}^{pp}$ and $\mathbf{C}^{pp}$ are in the form of $\langle \nabla\varphi, a\nabla\varphi \rangle_\Omega$, in which $\langle a, b \rangle_\Omega$ denotes the integration of

$a \cdot b$ over the computation domain Ω. a denotes the material parameter. $\mathbf{K}^{cc}$ is in the form of $\langle \nabla \times \Phi^c, \mu^{-1} \nabla \times \Phi^c \rangle_\Omega$. If ABC boundary is considered, the boundary integral term $\langle A, B \rangle_{\Gamma_{ABC}}$ will appear in $\mathbf{C}$. If lumped elements such as R, L, C are considered, the terms associated with them are added to the matrices $\mathbf{C}$, $\mathbf{K}$, and $\mathbf{M}$ respectively.

In the MFEM formulation based on tree-cotree splitting, the gradient matrix $\mathbf{G}$ is equal to $\begin{bmatrix} \mathbf{0} \\ \mathbf{I} \end{bmatrix}$, where $\mathbf{I}$ denotes the identity matrix. Substituting $\mathbf{G}$ into equation (5), it is easy to know that the constraint equation (5) is the same as the second matrix equation in wave equation (4), indicating that the wave equation automatically satisfies the constraint equation. So only the wave eqaution (4) needs to be solved in MFEM in the following three scenarios.

(a) Diffusion equation: For the diffusion equation with s^2 term disappeared in equation (4), the solution can be written as

$$\mathbf{e} = -s(s\mathbf{C} + \mathbf{K})^{-1}\mathbf{b} \tag{10}$$

(b) Lossless wave equation: Similarly, for the equation with s term disappeared in equation (4), the solution is

$$\mathbf{e} = -s(s^2\mathbf{M} + \mathbf{K})^{-1}\mathbf{b} \tag{11}$$

(c) Lossy wave equation: In equation (10) and (11), $\mathbf{M}$ and $\mathbf{C}$ are symmetric positive and non-negative definite matrices, respectively. $\mathbf{K}$ is symmetric and positive semi-definite. Symmetric Lanczos algorithm can be applied to solve $(s\mathbf{C}+\mathbf{K})^{-1}$ and $(s^2\mathbf{M} + \mathbf{K})^{-1}$, but it may not be able to solve $(s^2\mathbf{M} + s\mathbf{C} + \mathbf{K})^{-1}$ [16]. So the wave equation is reformulated to a pair of first order systems and are shown as follows

$$s\begin{bmatrix} \mathbf{C} & \alpha\mathbf{M} \\ \alpha\mathbf{M} & \mathbf{0} \end{bmatrix}\begin{bmatrix} \mathbf{e} \\ s\mathbf{e}' \end{bmatrix} + \begin{bmatrix} \mathbf{K} & \mathbf{0} \\ \mathbf{0} & -\alpha^2\mathbf{M} \end{bmatrix}\begin{bmatrix} \mathbf{e} \\ s\mathbf{e}' \end{bmatrix} = \begin{bmatrix} s\mathbf{b} \\ \mathbf{0} \end{bmatrix} \tag{12}$$

where $\mathbf{e}' = \mathbf{e}/\alpha$, α is a parameter to balance the order of magnitude of matrix elements. Let

$$\mathbf{M}' = \begin{bmatrix} \mathbf{C} & \alpha\mathbf{M} \\ \alpha\mathbf{M} & \mathbf{0} \end{bmatrix} \tag{13}$$

$$\mathbf{K}' = \begin{bmatrix} \mathbf{K} & \mathbf{0} \\ \mathbf{0} & -\alpha^2\mathbf{M} \end{bmatrix} \tag{14}$$

$\mathbf{M}'$ and $\mathbf{K}'$ are symmetric but indefinite. In this paper, equation (12) is solved by the modified symmetric Lanczos method which will be discussed later and the solution is given by

$$\begin{bmatrix} \mathbf{e} \\ s\mathbf{e}' \end{bmatrix} = -s(s\mathbf{M}' + \mathbf{K}')^{-1}\begin{bmatrix} \mathbf{b} \\ \mathbf{0} \end{bmatrix} \tag{15}$$

III. SYMMETRIC LANCZOS ALGORITHM

Symmetric Lanczos algorithm is an effective MOR approach to approximate the broadband matirx transfer functions in (10), (11) and (15). Since equations (10), (11) have the same form, without loss of generality, with equation (11) as an example, the corresponding eigenvalue problem is

$$(\mathbf{K} - s_0^2\mathbf{M})^{-1}\mathbf{M}x = \frac{1}{\lambda - \sigma}x \tag{16}$$

where s_0^2 is an offset to make $\mathbf{K} - s_0^2\mathbf{M}$ nonsingular. Let $\mathbf{A} = \mathbf{K} - s_0^2\mathbf{M}$, $\mathbf{B} = \mathbf{A}^{-1}\mathbf{M}$. For nonsymmetric matrix $\mathbf{B}$, two sided Lanczos ailgorithm should be employed. Reference [31] points out that the symmetric Lanczos algorithm can be applied to $\mathbf{B}$ by taking the advantage of its self-adjoint property with respect to the $\mathbf{M}$ inner product. But it is required that $\mathbf{M}$ must be positive definite or positive semi-definite to ensure the inner product $\mathbf{y}^T\mathbf{M}\mathbf{y}$ always positve or zero for any choice of $\mathbf{y}$. The symmetric Lanczos algorithm is given in Algorithm 1.

Algorithm 1 The Symmetric Lanczos Algorithm

1: Initialize $\mathbf{r} = \mathbf{A}^{-1}\mathbf{b}$; $\beta(1) = \sqrt{\mathbf{r}^T\mathbf{M}\mathbf{r}}$; $\mathbf{r} = \frac{\mathbf{r}}{\beta(1)}$; $\mathbf{q}_0$=zeros(dim($\mathbf{A}$),1);
2: **for** $i = 1$ to k **do**
3: $\quad \mathbf{Q}(i) = \mathbf{r}$;
4: $\quad \mathbf{p} = \mathbf{M}\mathbf{r}$;
5: $\quad$ Remove spurious modes by enforcing $\mathbf{G}^T\mathbf{p} = 0$;
6: $\quad \mathbf{r} = \mathbf{A}^{-1}\mathbf{p}$;
7: $\quad \alpha(i) = \mathbf{r}^T\mathbf{p}$;
8: $\quad \mathbf{r} = \mathbf{r} - \alpha(i)\mathbf{Q}(i) - \beta(i)\mathbf{q}_0$;
9: $\quad \beta(i+1) = \sqrt{\mathbf{r}^T\mathbf{M}\mathbf{r}}$;
10: $\quad \mathbf{r} = \frac{\mathbf{r}}{\beta(i+1)}$;
11: $\quad \mathbf{q}_0 = \mathbf{Q}(i)$;
12: **end for**

The constrint equation (5) is implemented in line 5 in the symmetric Lanczos algorithm. The symmetric Lanczos algorithm can be summarized as a three-term recurrences

$$\mathbf{B}\mathbf{Q} = \mathbf{Q}\mathbf{T} \tag{17}$$

where $\mathbf{Q} = [\mathbf{q}_1, \mathbf{q}_2, \cdots, \mathbf{q}_k]$ satisfies the othogonality condition

$$\mathbf{Q}^T\mathbf{Q} = \mathbf{I} \tag{18}$$

$\mathbf{T}$ is the symmetric tridiagonal matrix given by

$$\mathbf{T} = \begin{bmatrix} \alpha_1 & \beta_2 & & & \\ \beta_2 & \alpha_2 & \beta_3 & & \\ & \beta_3 & \ddots & \ddots & \\ & & \ddots & \ddots & \beta_k \\ & & & \beta_k & \alpha_k \end{bmatrix} \tag{19}$$

Following the procedure in reference [10], the weighted residual method is used to construct the approximate solution of equation (11). Expanding the unknown vector $\mathbf{e}$ by Lanczos vectors, we obtain

$$\mathbf{e} = \sum_{i=1}^{k} \mathbf{q}_i w_i = \mathbf{Q}\mathbf{w} \tag{20}$$

where $\mathbf{w} = [w_1, w_2, \cdots, w_k]$ is the coefficient vector. Substituting (20) into (11), the residual vector is given by

$$\mathbf{d} = [\mathbf{I} + (s_0^2 + s^2)\mathbf{B}]\mathbf{Q}\mathbf{w} + s\mathbf{A}^{-1}\mathbf{b} \tag{21}$$

Making use of the orthogonality between the residual vector $\mathbf{d}$ and the columns of $\mathbf{Q}^T$ and equations (17) - (18), we obtain

$$\mathbf{w} = -s[\mathbf{I} + (s_0^2 + s^2)\mathbf{T}]^{-1}\mathbf{Q}^T\mathbf{A}^{-1}\mathbf{b} \tag{22}$$

Since the starting Lanczos vector $\mathbf{q}_1$ is chosen to be $\mathbf{A}^{-1}\mathbf{b}$ in the Lanczos algorithm, the solution of (20) is finally approximated by the following reduced equation

$$\mathbf{e} = -s\beta_1\mathbf{Q}\mathbf{V}[\mathbf{I} + (s_0^2 + s^2)\Lambda]^{-1}\mathbf{V}^T\mathbf{e}_1 \tag{23}$$

where $\mathbf{T} = \mathbf{V}\Lambda\mathbf{V}^T$, representing the spectral decomposition of $\mathbf{T}$. Λ is a diagonal matrix and $\mathbf{e}_1$ is the first column of the identity matrix.

In the symmetric Lanczos method, matrix $\mathbf{A}$ is factorized once. The high-frequency error of the solution can be improved by increasing the number of iterations. Then a spectral decomposition of a small scale tridiagonal matrix is performed once to obtain the expression of the whole frequency band.

Since $\mathbf{M}'$ is indefinite in equation (15), the symmetric Lanczos method mentioned above may fail. Reference [10] solves the problem by modifying the two sided Lanczos algorithm by taking the advantage of the symmetry of $\mathbf{M}'$ and $\mathbf{K}'$. Let $\mathbf{A} = \mathbf{K}' - s_0\mathbf{M}'$, $\mathbf{B} = \mathbf{A}^{-1}\mathbf{M}'$, the three-term recurrences for the two sided Lanczos algorithm are given as follows

$$\mathbf{B}\mathbf{Q} = \mathbf{Q}\mathbf{U}^{-1}\mathbf{T} \tag{24}$$

$$\mathbf{P}^T\mathbf{B} = \mathbf{T}\mathbf{U}^{-1}\mathbf{P}^T \tag{25}$$

where $\mathbf{P} = [\mathbf{p}_1, \mathbf{p}_2, \cdots, \mathbf{p}_k]$ and $\mathbf{Q} = [\mathbf{q}_1, \mathbf{q}_2, \cdots, \mathbf{q}_k]$ are left Lanczos vectors and right Lanczos vectors, respectively. They satisfy the bi-othogonality condition

$$\mathbf{P}^T\mathbf{Q} = \mathbf{U} \tag{26}$$

where $\mathbf{U}$ = diag $(v_1, v_2, \ldots, v_k)$, the entries on the diagonal are either 1 or -1. $\mathbf{T}$ is the tridiagonal matrix given by

$$\mathbf{T} = \begin{bmatrix} \alpha_1 & \beta_2 & & & \\ \gamma_2 & \alpha_2 & \beta_3 & & \\ & \gamma_3 & \ddots & \ddots & \\ & & \ddots & \ddots & \beta_k \\ & & & \gamma_k & \alpha_k \end{bmatrix} \tag{27}$$

In reference [10], it is shown that when $\mathbf{P}$ is chosen to be $\mathbf{M}'\mathbf{Q}$, the tridiagonal matrix $\mathbf{T}$ will be symmetric, that is $\beta_i = \gamma_i$ $(i = 2, \ldots k)$. This modified symmetric Lanczos algorithm is shown in Algorithm 2. The constraint equation (5) is implemented in line 13 by refering to [32]. Here $\mathbf{G}$ is the nullspace of stiffness matrix and $\widetilde{\mathbf{G}}$ consists of the columns of $\mathbf{G}$ associated with internal nodes which are in passive and lossless regions.

By using the weighted residual method mentioned above, we can obtain the solution of equation (15)

$$\mathbf{e} = -s\beta_1\mathbf{Q}[\mathbf{U} + (s_0 + s)\mathbf{T}]^{-1}\mathbf{e}_1 \tag{28}$$

Algorithm 2 The Modified Symmetric Lanczos Algorithm

1: Initialize $\mathbf{r} = \mathbf{A}^{-1}\mathbf{b}$; temp=$\mathbf{r}^T\mathbf{M}'\mathbf{r}$; $\beta(1) = \sqrt{|temp|}$;
2: **if** temp< 0 **then**
3: $\quad v(1) = -1$;
4: **else**
5: $\quad v(1) = 1$;
6: **end if**
7: $\mathbf{r} = v(1) \cdot \frac{\mathbf{r}}{\beta(1)}$;
8: $\mathbf{q}_0 =$ zeros(dim($\mathbf{A}$),1);
9: $v_0 = 1$;
10: **for** $i = 1$ to k **do**
11: $\quad \mathbf{Q}(i) = \mathbf{r}$;
12: $\quad \mathbf{p} = \mathbf{M}'\mathbf{r}$;
13: $\quad$ Remove spurious modes by enforcing $\mathbf{p}$ with $\begin{bmatrix} \mathbf{G}^T & \mathbf{0} \\ \mathbf{0} & \widetilde{\mathbf{G}}^T \end{bmatrix} \cdot \mathbf{p} = 0$;
14: $\quad \mathbf{r} = \mathbf{A}^{-1}\mathbf{p}$;
15: $\quad \mathbf{r} = \mathbf{r} - \beta(i)\mathbf{q}_0/v_0$;
16: $\quad \alpha(i) = \mathbf{r}^T\mathbf{p}$;
17: $\quad \mathbf{r} = \mathbf{r} - \alpha(i)\mathbf{Q}(i)/v(k)$;
18: $\quad$ temp $= \mathbf{r}^T\mathbf{M}'\mathbf{r}$;
19: $\quad \beta(i+1) == \sqrt{|temp|}$;
20: $\quad$ **if** temp< 0 **then**
21: $\quad\quad v(i+1) = -1$;
22: $\quad$ **else**
23: $\quad\quad v(i+1) = 1$;
24: $\quad$ **end if**
25: $\quad \mathbf{r} = v(i+1) \cdot \frac{\mathbf{r}}{\beta(i+1)}$;
26: $\quad \mathbf{q}_0 = \mathbf{Q}(i)$;
27: $\quad v_0 = v(i)$;
28: **end for**

Compared to discrete frequency sweep method, in which a large-scale sparse linear equation need to be solved at each frequency, the modified symmetric Lanczos algorithm employed here is a fast frequency sweep method that by one matrix inversion, the field in the entire frequency band is obtained rapidly by solving the reduced order matrix equation. In equation (23), the solution within the whole frequency band can be obtained by one spectral decomposition of the small-scale tridiagonal matrix $\mathbf{T}$. Different from that, since $\mathbf{U}$ in (28) is not the identity matrix, spectral decomposition cannot be used and the inverse of the small-scale tridiagonal matrix needs to be obtained at each frequency point.

IV. NUMERICAL EXPERIMENTS AND DISCUSSIONS

In this section, two IPD filters and an interconnect model are simulated to verify the new fast sweep frequency method based on the symmetric Lanczos algorithm and MFEM mehtod, called MFEM-SymLanc in this paper. The results of HFSS with fast sweep and interpolation sweep are used for comparison. Since the mesh quality has a great influence on the broadband simulation for complex multiscale models, in order to eliminate the influence of mesh quality, we use the

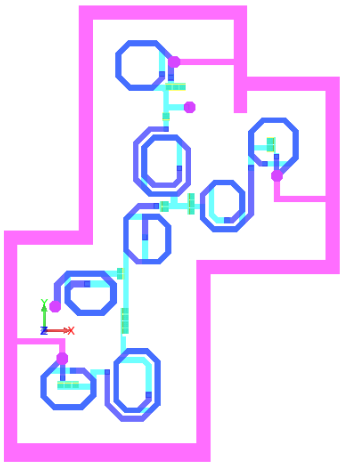

FIGURE 1. The top view of the first IPD filter.

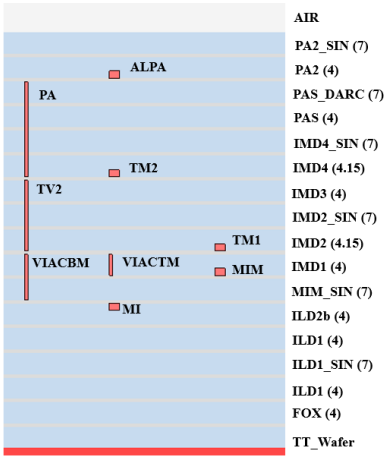

FIGURE 2. The laminated structure of the first IPD filter.

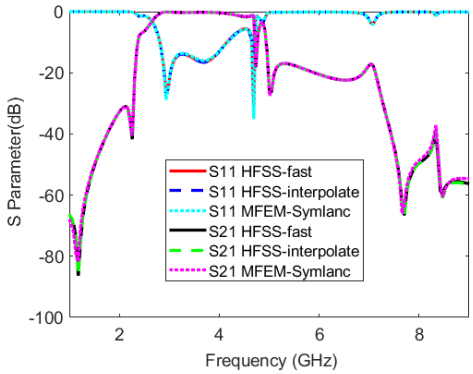

FIGURE 3. S parameters calculated by MFEM-SymLanc and HFSS with fast sweep.

same linear tetrahedron elements generated from HFSS and the second order basis functions for MFEM-SymLanc and HFSS. Since the adaptive passes for meshing consume a large amount of time in HFSS, the meshing time is not included in the CPU time in HFSS for a reasonable comparison with MFEM-SymLanc method. The simulation is performed on a server with two Intel(R) Xeon(R) X5690 CPUs at 3.46 GHz and 192 GB memory. 40 cores are used for parallel simulation in HFSS. Direct solver MUMPUS is adopted for matrix inversion in the MFEM-SymLanc method.

A. IPD FILTERS

In the first example, a IPD filter with seventeen dielectric substrates, vias and metal traces is analyzed. The top view and the laminated structure are shown in Fig. 1 and Fig. 2. Fig. 2 defines the position of dielectric layers and the relative permittivity of layers are in parentheses. Conductors and vias are represented by the red parts. The total size of the IPD filter is $1842.813 \times 2322.376 \times 284.311\ \mu\text{m}^3$. Two lumped ports are loaded with 50 Ω resistors. In the simulation, the model is truncated by the radiation boundary, except for the metal substrate on the bottom. The conductors embedded in the dielectric substrates are modeled as PEC. Algorithm 2 is adopted in the MFEM-SymLanc method since there are both s^2 term and s term in the equation when resistors and radiation boundary are present. The frequency range for this filter is 1 - 9 GHz and 200 frequency points are simulated. The filter is discretized into 486037 tetrahedron elements by HFSS.

The calculated S parameters by MFEM-SymLanc and HFSS with fast sweep and interpolation sweep are shown in Fig. 3. As can be seen, the results of the three methods agree very well. 100 Lanczos vectors are used in the MFEM-SymLanc method, in other words, the number of iterations in Algorithm 2 is 100. The computation time and memory consumption of the three methods are compared in Table 1. It can be seen that when the order of basis functions and mesh are the same, the degrees of freedom (DoF) of HFSS and MFEM-SymLanc are nearly the same. The reason for the difference is that the two solvers model the lumped port differently. It is clear that the MFEM-SymLanc method is the most efficient among the three methods. Since the fast frequency sweep method in HFSS-fast solver is also based on the Lanczos algorithm, it is more efficient than the interpolation algorithm in HFSS-interpolate solver. The memory consumption of HFSS-fast and MFEM-SymLanc is almost the same. Since HFSS-interpolate solves multiple frequencies in parallel, it consumes much more memory than the other two methods.

Next, the above IPD filter is used to compare the MFEM-SymLanc method with the MFETD method in [20], [25], and [26]. Since the authors has proved in [25] that MFETD based on tree-cotree splitting [25], [26] is more efficient than MFETD based on Lagrangian multiplier [20], so here we will compare the accuracy and efficiency of the MFEM-SymLanc method and the MFETD in [25] and [26]. The calculated S parameters by the two methods are shown in Fig. 4. And the total voltages at the two ports calculated by MFETD are shown in Fig. 5. In [25] and [26], an implicit time-stepping scheme is used for electrical small problems. In this example, the time sampling rate is 20 points per period. Since PEC

TABLE 1. Computational resources of the first IPD filter by MFEM-SymLanc, HFSS and MFETD.

Method	DoF	Time	Speedup	Memory (GB)
HFSS-interpolate	2958374	2 h	1	171
HFSS-fast	2958374	23 min	5.2	42.2
MFEM-SymLanc	2960636	5.8 min	20.7	42.6
MFETD	2960636	154 min	−−	42.6

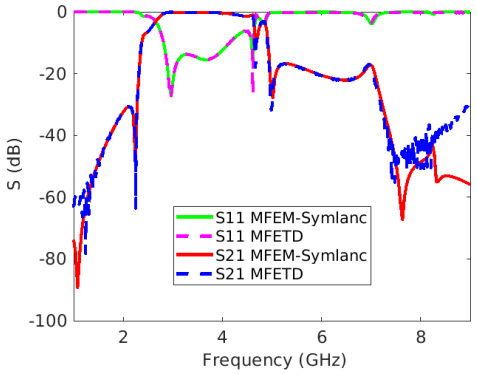

FIGURE 4. S parameters calculated by MFEM-SymLanc and MFETD.

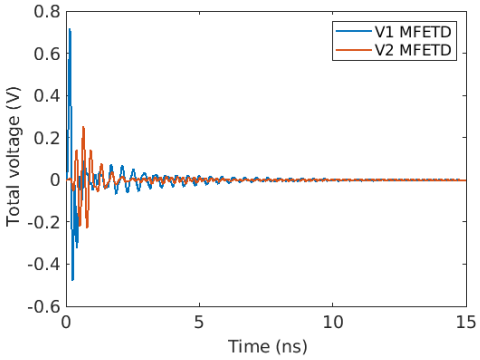

FIGURE 5. The total voltages calculated by the MFETD method.

is used to simulate metal in the model, even if the runtime is 135 periods (corresponding to the maximum frequency), the energy still has not decayed to 0. The voltages are still oscillating at 15 ns, so the S parameters calculated by the Fourier transform in MFETD are not as accurate as MFEM-SymLanc. And it can be seen from Table 1 that the calculation time of MFETD is 154 minutes, which is much higher than the time in the MFEM-SymLanc method. This is mainly because it is quite time-consuming in a large loop to call the results produced by LU decomposition in MUMPUS. In the MFETD method, the LU decomposition using MUMPUS takes about 2 minutes, while it takes about 150 minutes when call the LU decomposition results in 2700 time steps. However, in the MFEM-SymLanc method, the number of loops to call the LU factorization results is determined by k in Algorithm 2 (chosen as 100 in this example), which is much smaller than the number of time steps, so the

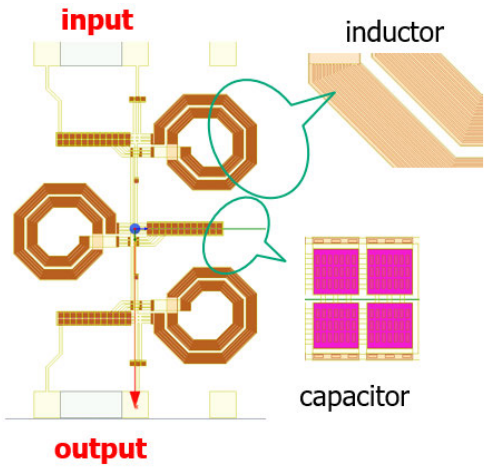

FIGURE 6. The top view of the second IPD filter.

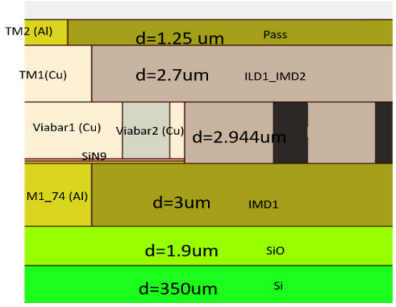

FIGURE 7. The side view of the second IPD filter.

MFEM-SymLanc method is much more efficient and accurate than the MFETD method in [25] and [26].

Then the second IPD filter is analyzed with the top view and side view shown in Fig. 6 and Fig. 7. The filter consists of 6 layers of dielectric substrates and 2486 entities. The total size is $2500 \times 2000 \times 361.794\ \mu\text{m}^3$ and the width of the smallest coil is only 2 μm. The frequency range for this filter is 0.1 - 10 GHz and 110 frequency points are simulated. The filter is discretized into 494117 tetrahedron elements by HFSS. 50 Lanczos vectors are used in the MFEM-SymLanc method.

The results obtained by MFEM-SymLanc and HFSS with fast sweep and interpolation sweep are shown in Fig. 8. Compared with the HFSS-interpolation solver and MFEM-SymLanc method, the result of HFSS-fast solver at low frequency band is inaccurate. The reason for the inaccuracy is probably caused by the inaccurate Lanczos vectors calculated in the HFSS-fast solver. Furthermore, the mixed finite element method adopted by MFEM-SymLanc removes spurious modes and ensures accuracy of low frequency results. The computation time, DoFs and memory consumption of the three methods are also given in Table 2. Compared with the interpolation sweep, the CPU time speedup of the HFSS-fast solver and the MFEM-SymLanc are 2 and 16, respectively. It is clear that the proposed MFEM-SymLanc method is much more efficient and accurate than the HFSS-fast solver for wideband simulation.

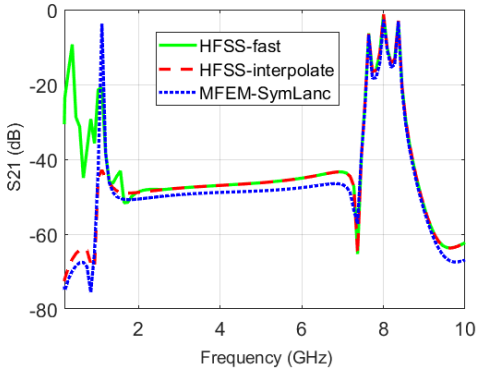

FIGURE 8. S parameters calculated by MFEM-SymLanc and HFSS with fast sweep and interpolate sweep.

TABLE 2. Computational resources of the second IPD filter by MFEM-SymLanc and HFSS.

Method	DoF	Time	Speedup	Memory (GB)
HFSS-interpolate	2753500	74 min	1	114
HFSS-fast	2753500	37 min	2	24.3
MFEM-SymLanc	2754100	4.6 min	16	27.2

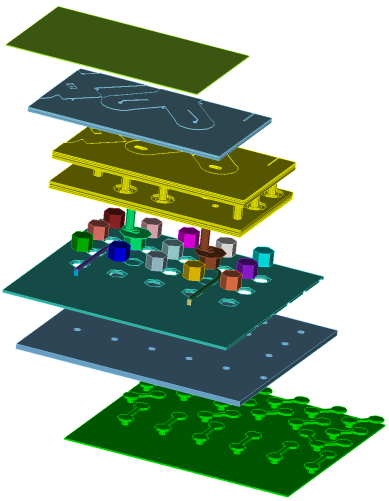

FIGURE 9. 3D model of the interconnect model.

B. INTERCONNECT MODEL

An interconnect model with multilayer substrates and four lumped ports shown in Fig. 9 is analyzed to verify the efficiency of the MFEM-SymLanc method. The relative dielectric constant of the dielectric substrates is 4.4 and the conductors embedded in the substrates is modeled as PEC. The total size of the model is $6.6 \times 6.6 \times 1.8$ mm^3. Radiation boundary with the airbox of size $8 \times 8 \times 2.8$ mm^3 is used to truncate the model. A wideband 30 MHz - 10 GHz is studied and 200 frequency points are simulated. The interconncet model is discretized into 203896 tetrahedron elements by HFSS.

To ensure the accuracy of high frequency results, 500 Lanczos vectors are used in the MFEM-SymLanc method. The results obtained by MFEM-SymLanc and HFSS

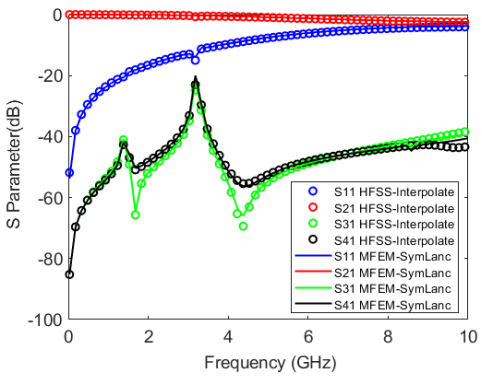

FIGURE 10. S parameters calculated by MFEM-SymLanc and HFSS with interpolation sweep.

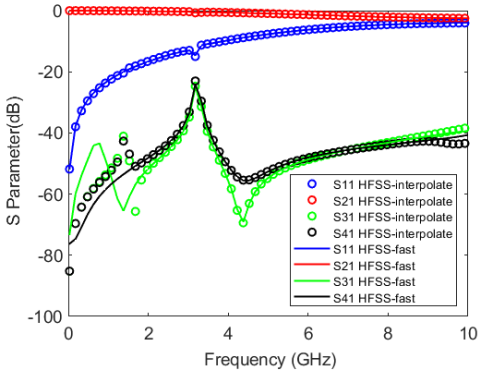

FIGURE 11. S parameters calculated by HFSS with interpolation sweep and fast sweep.

TABLE 3. Computational resources of interconnect model by MFEM-SymLanc and HFSS.

Method	DoF	Time	Speedup	Memory (GB)
HFSS-interpolate	1179056	20 min	1	47.9
HFSS-fast	1179056	12 min	1.7	7.37
MFEM-SymLanc	1179840	6.5 min	3	16.3

with fast sweep and interpolation sweep are shown in Fig. 10 and Fig. 11. Generally, interpolation sweep are more accurate than fast sweep for wideband simulation in HFSS, but less efficient. It can be seen from Fig. 11 that the result of fast sweep has a large error when the frequency is lower than 2 GHz; in Fig. 10, the result of MFEM-SymLanc shows high accuracy from 30 MHz to 10 GHz, because the mixed finite element method adopted by MFEM-SymLanc guarantees high accuracy in low frequency band. In addition, the computation time, DoFs and memory consumption of the three methods are also given in Table 3. Taking the result of interpolation sweep as the reference, the method proposed in this paper is 3 times faster while the fast sweep solver is 1.7 times faster than it, but the fast sweep solver has lower accuracy at low frequencies. In this model, MFEM-SymLanc consumes more memory than HFSS-fast.

V. CONCLUSION

The mixed finite element method and symmetric Lanczos algorithm are combined to simulate three real-life 3-D PCB models in this paper. Two kinds of symmetric Lanczos algorithm are employed to EM equations with different combinations of s and s^2 term. The results show that the proposed method is more efficient than the interpolation solver and fast solver in HFSS, and has higher accuracy than the fast solver in HFSS at low frequencies. The hybrid method has advantages on the simulation of electrical small model with multilayered interconnect structures with fewer iterations in the symmetric Lanczos algorithm. As the frequency increases, more iterations are needed to approximate the electromagnetic field distribution of the original problem. So one difficulty of this method is to determine the number of iterations for different models. In the future, we will continue to study how to automatically select the appropriate number of iterations to ensure the high accuracy and efficiency.

REFERENCES

[1] R. D. Slone, J.-F. Lee, and R. Lee, "A comparison of some model order reduction techniques," *Electromagnetics*, vol. 22, no. 4, pp. 275–289, May 2002.
[2] J. E. Bracken, D.-K. Sun, and Z. Cendes, "Characterization of electromagnetic devices via reduced-order models," *Comput. Methods Appl. Mech. Eng.*, vol. 169, nos. 3–4, pp. 311–330, Feb. 1999.
[3] Z. Q. Qu, *Model Order Reduction Techniques With Applications in Finite Element Analysis*. London, U.K.: Springer, 2013.
[4] L. Komzsik, *The Lanczos Method: Evolution and Application*. Philadelphia, PA, USA: SIAM, 2003.
[5] J. E. Bracken, V. Raghavan, and R. A. Rohrer, "Interconnect simulation with asymptotic waveform evaluation (AWE)," *IEEE Trans. Circuits Syst. I, Fundam. Theory Appl.*, vol. 39, no. 11, pp. 869–878, Nov. 1992.
[6] S. K. Das and W. T. Smith, "Application of asymptotic waveform evaluation for analysis of skin effect in lossy interconnects," *IEEE Trans. Electromagn. Compat.*, vol. 39, no. 2, pp. 138–146, May 1997.
[7] R. D. Slone, R. Lee, and J.-F. Lee, "Multipoint Galerkin asymptotic waveform evaluation for model order reduction of frequency domain FEM electromagnetic radiation problems," *IEEE Trans. Antennas Propag.*, vol. 49, no. 10, pp. 1504–1513, Oct. 2001.
[8] R. D. Slone, R. Lee, and J.-F. Lee, "Well-conditioned asymptotic waveform evaluation for finite elements," *IEEE Trans. Antennas Propag.*, vol. 51, no. 9, pp. 2442–2447, Sep. 2003.
[9] L. T. Pillage and R. A. Rohrer, "Asymptotic waveform evaluation for timing analysis," *IEEE Trans. Comput.-Aided Design Integr. Circuits Syst.*, vol. 9, no. 4, pp. 352–366, Apr. 1990.
[10] B. Nour-Omid and M. E. Regelbrugge, "Lanczos method for dynamic analysis of damped structural systems," *Earthq. Eng. Struct. Dyn.*, vol. 18, no. 8, pp. 1091–1104, Nov. 1989.
[11] D. Day, "An efficient implementation of the nonsymmetric Lanczos algorithm," *SIAM J. Matrix Anal. Appl.*, vol. 18, no. 3, pp. 566–589, Jul. 1997.
[12] S. V. Polstyanko, R. Dyczij-Edlinger, and J.-F. Lee, "Fast frequency sweep technique for the efficient analysis of dielectric waveguides," *IEEE Trans. Microw. Theory Techn.*, vol. 45, no. 7, pp. 1118–1126, Jul. 1997.
[13] D. K. Sun, "ALPS: An adaptive Lanczos–Padé spectral solution of mixed-potential integral equation," *Comput. Methods Appl. Mech. Eng.*, vol. 169, nos. 3–4, pp. 432–452, Feb. 1999.
[14] D.-K. Sun, Z. Cendes, and J.-F. Lee, "ALPS—A new fast frequency-sweep procedure for microwave devices," *IEEE Trans. Microw. Theory Techn.*, vol. 49, no. 2, pp. 398–402, Feb. 2001.
[15] M. R. Zunoubi, K. C. Donepudi, J. M. Jin, and W. C. Chew, "Efficient time-domain and frequency-domain finite-element solution of Maxwell's equations using spectral Lanczos decomposition method," *IEEE Trans. Microw. Theory Techn.*, vol. 34, no. 4, pp. 346–347, Aug. 1998.
[16] R. D. Slone and R. Lee, "Applying Padé via Lanczos to the finite element method for electromagnetic radiation problems," *Radio Sci.*, vol. 35, no. 2, pp. 331–340, Mar. 2000.
[17] F. Feng, J. Zhang, J. Jin, W. Zhang, Z. Zhao, and Q.-J. Zhang, "Adjoint EM sensitivity analysis for fast frequency sweep using matrix Padé via Lanczos technique based on finite-element method," *IEEE Trans. Microw. Theory Techn.*, vol. 69, no. 5, pp. 2413–2428, May 2021.
[18] D. Sun, J. Manges, X. Yuan, and Z. Cendes, "Spurious modes in finite-element methods," *IEEE Antennas Propag. Mag.*, vol. 37, no. 5, pp. 12–24, Oct. 1995.
[19] N. V. Venkatarayalu and J.-F. Lee, "Removal of spurious DC modes in edge element solutions for modeling three-dimensional resonators," *IEEE Trans. Microw. Theory Techn.*, vol. 54, no. 7, pp. 3019–3025, Jul. 2006.
[20] K. Chen, X. Hou, M. Zhuang, N. Liu, and Q. H. Liu, "An efficient mixed finite-element time-domain method for complex electrically small problems," *IEEE Trans. Microw. Theory Techn.*, vol. 67, no. 4, pp. 1285–1294, Apr. 2019.
[21] S.-H. Lee and J.-M. Jin, "Application of the tree-cotree splitting for improving matrix conditioning in the full-wave finite-element analysis of high-speed circuits," *Microw. Opt. Technol. Lett.*, vol. 50, no. 6, pp. 1476–1481, Jun. 2008.
[22] J. Zhu and D. Jiao, "Fast full-wave solution that eliminates the low-frequency breakdown problem in a reduced system of order one," *IEEE Trans. Compon., Packag., Manuf. Technol.*, vol. 2, no. 11, pp. 1871–1881, Nov. 2012.
[23] R. Wang, D. J. Riley, and J.-M. Jin, "Application of tree-cotree splitting to the time-domain finite-element analysis of electromagnetic problems," *IEEE Trans. Antennas Propag.*, vol. 58, no. 5, pp. 1590–1600, May 2010.
[24] J. Ma, J.-M. Jin, and Z. Nie, "A nonconformal FEM-DDM with tree-cotree splitting and improved transmission condition for modeling subsurface detection problems," *IEEE Trans. Geosci. Remote Sens.*, vol. 52, no. 1, pp. 355–364, Jan. 2014.
[25] K. Chen, J. Liu, M. Zhuang, Q. Sun, and Q. H. Liu, "New mixed SETD and FETD methods to overcome the low-frequency breakdown problems by tree-cotree splitting," *IEEE Trans. Microw. Theory Techn.*, vol. 68, no. 8, pp. 3219–3228, Aug. 2020.
[26] K. Chen, M. Zhuang, J. Liu, M. Yuan, and Q. H. Liu, "A combination of mixed FETD method and SPICE to simulate nonlinear multiport circuits," *IEEE Microw. Wireless Compon. Lett.*, vol. 31, no. 2, pp. 97–100, Feb. 2021.
[27] K. Fumio, "Mixed and penalty formulations for finite element analysis of an eigenvalue problem in electromagnetism," *Comput. Methods Appl. Mech. Eng.*, vol. 64, nos. 1–3, pp. 509–521, Oct. 1987.
[28] Y. Zhou, L. Shi, N. Liu, C. Zhu, Y. Sun, and Q. H. Liu, "Mixed spectral-element method for overcoming the low-frequency breakdown problem in subsurface em exploration," *IEEE Trans. Geosci. Remote Sens.*, vol. 55, no. 6, pp. 3488–3500, Jun. 2017.
[29] N. Liu, L. E. Tobón, Y. Zhao, Y. Tang, and Q. H. Liu, "Mixed spectral-element method for 3-D Maxwell's eigenvalue problem," *IEEE Trans. Microw. Theory Techn.*, vol. 63, no. 2, pp. 317–325, Feb. 2015.
[30] R. Hong, K. Chen, X. Hou, Q. Sun, N. Liu, and Q. H. Liu, "Mixed finite element method for full-wave simulation of bioelectromagnetism from DC to microwave frequencies," *IEEE Trans. Biomed. Eng.*, vol. 67, no. 10, pp. 2765–2772, Oct. 2020.
[31] B. N. Parlett and H. C. Chen, "Use of indefinite pencils for computing damped natural modes," *Linear Algebra Appl.*, vol. 140, pp. 53–88, Oct. 1990.
[32] S. J. Wang, J. Liu, M. W. Zhuang, K. Chen, and Q. H. Liu, "Mixed spectral-element methods for 3-D Maxwell's eigenvalue problems with Bloch periodic and open resonators," *IEEE Trans. Microw. Theory Techn.*, vol. 69, no. 3, pp. 1547–1558, Mar. 2021.

KE CHEN (Member, IEEE) received the B.S. degree in industrial engineering and the M.S. degree in mechanical engineering from the University of Electronic Science and Technology of China, Chengdu, China, in 2013 and 2016, respectively, and the Ph.D. degree in electromagnetic field and microwave technology from Xiamen University, in 2020. She is currently a Postdoctoral Researcher with Xiamen University. Her research interests include computational electromagnetics, IC simulation, and multiscale computing.

JUNHUI CHEN received the B.S. degree in engineering from Hubei Normal University, China, in 2019. He is currently pursuing the M.S. degree with Xiamen University, China. His research interest includes computational electromagnetism, focusing on the fast and effective solution of field circuit coupling problems.

XUANYING HOU received the B.S. and M.S. degrees in engineering from Xiamen University, China, in 2016 and 2019, respectively, where she is currently pursuing the Ph.D. degree. Her research interest includes computational electromagnetics, with a focus on the fast and efficient methods for geological problems.

MINGWEI ZHUANG (Member, IEEE) received the B.S. degree in applied physics from the University of Shandong Jiaotong of China, Jinan, China, in 2011, and the Ph.D. degree in radiophysics from the Institude of Electromagnetics and Acoustics, Xiamen University, Xiamen, China, in 2019. From 2016 to 2017, he was a Visiting Student at the Department of Electrical and Computer Engineering, Duke University, Durham, NC, USA. His research interests include numerical methods in acoustics, electromagnetics, and multiphysics field.

QING HUO LIU (Fellow, IEEE) received the B.S. and M.S. degrees in physics from Xiamen University, Xiamen, China, in 1983 and 1986, respectively, and the Ph.D. degree in electrical Engineering from the University of Illinois at Urbana–Champaign, Champaign, IL, USA, in 1989.

He was a Research Assistant at the Electromagnetics Laboratory, University of Illinois at Urbana-Champaign, from September 1986 to December 1988, and a Postdoctoral Research Associate, from January 1989 to February 1990. He was a Research Scientist and a Program Leader at the Schlumberger-Doll Research, Ridgefield, CT, USA, from 1990 to 1995. From 1996 to May 1999, he was an Associate Professor at New Mexico State University, Las Cruces, NM, USA. From 1999 to 2022, he was a tenured Full Professor of electrical and computer engineering with Duke University, Durham, NC, USA. He is currently a Chair Professor with the Eastern Institute for Advanced Study and a Visiting Chair Professor with Xiamen University. His research interests include computational electromagnetics and acoustics, inverse problems, and their application in nanophotonics, geophysics, biomedical imaging, and electronic design automation. He has published widely in these areas.

Dr. Liu is a fellow of the Optical Society of America, the Acoustical Society of America, and the Electromagnetics Academy. He received the 1996 Presidential Early Career Award for Scientists and Engineers (PECASE) from the White House, the 1996 Early Career Research Award from the Environmental Protection Agency, and the 1997 CAREER Award from the National Science Foundation. He received the 2017 Technical Achievement Award, the 2018 Computational Electromagnetics Award from the Applied Computational Electromagnetics Society, the 2018 Harrington-Mittra Award in Computational Electromagnetics from the IEEE Antennas and Propagation Society, and the ECE Distinguished Alumni Award from the University of Illinois at Urbana–Champaign in 2018. He served as an IEEE Antennas and Propagation Society Distinguished Lecturer and the Founding Editor-in-Chief for the IEEE JOURNAL ON MULTISCALE AND MULTIPHYSICS COMPUTATIONAL TECHNIQUES, from 2015 to 2018.